Study of the dielectric properties of $ACu_3Ti_4O_{12}$ ($A = Eu_{2/3}$, $Tb_{2/3}$, and $Na_{1/2}Eu_{1/2}$)

M. Li,[a] Y. Shen, and C. X. Li
Department of Applied Physics, Xi'an University of Technology, Xi'an 710054, China

(Received 2 July 2019; accepted 24 August 2019)

We report the dielectric properties of $ACu_3Ti_4O_{12}$ ($A = Eu_{2/3}$, $Tb_{2/3}$, and $Na_{1/2}Eu_{1/2}$) (ACTO) in the frequency range of 40 Hz–2.5 MHz and in the temperature range of 293–473 K. The experimental results show that substituting for Ca improves the loss tangent of $CaCu_3Ti_4O_{12}$ (CCTO). Although the dielectric constants largely decrease, they remain at a high level of 10^3. To identify the observed dielectric performances of ACTO, scanning electron microscopy and complex impedance measurements were conducted. The conducting mechanism for the grain of ACTO was found to be ion jumping rather than electron hopping (for the grain of CCTO). The results show that the decreased dielectric constant may be related to the decreased grain size, the different carrier in the grain, the different grain boundary properties, or a combination of these factors. All these factors are associated with the deficiency of oxygen vacancies in the samples of ACTO. The decreased loss tangent may be due to the increase in the grain boundary resistance. © *2019 International Centre for Diffraction Data*. [doi:10.1017/S0885715619000769]

Key words: $CaCu_3Ti_4O_{12}$, microstructure, dielectric properties, oxygen vacancy

I. INTRODUCTION

Electroceramics with ultrahigh dielectric constant have triggered an extensive research because of their potential application in miniaturized electronic components/device. Recently, much attention has been paid to a body-centered cubic $CaCu_3Ti_4O_{12}$ (CCTO) as it exhibits high dielectric constant of 10^4–10^5 and good stability over a wide temperature range of 100–400 K (Subramanian *et al*., 2000; Homes *et al*., 2001; Sinclair *et al*., 2002; Wang and Zhang, 2007). In addition, CCTO is a lead-free (Pb-free) compound and thus does not cause environmental pollution. Theoretical calculations reveal that CCTO provides a dielectric constant only in the range of 40–50 (He *et al*., 2002). Impedance spectroscopy study on CCTO ceramics shows that they are electrically heterogeneous and consist of semiconducting grains with insulating grain boundaries. Therefore, an internal barrier layer capacitance (IBLC) model instead of an intrinsic property associated with the crystal structure (Capsoni *et al*., 2004; Fang and Liu, 2005; Zhang *et al*., 2005; Wang and Zhang, 2007) is suggested to be responsible for the giant dielectric constant of CCTO. Although this model is now generally accepted, the origin of semiconductivity in grain and the composition of the insulating grain boundary phase in CCTO ceramics are controversial. Furthermore, the loss tangent of CCTO is rather high (~0.1–0.2 at 1 kHz) from an application viewpoint. Improvements are therefore needed to facilitate device implementation.

It is intriguing to note that substituting for Ca usually decreases the ultrahigh dielectric constant of CCTO (Subramanian and Sleight, 2002; Homes *et al*., 2003; Liu *et al*., 2004, 2005; Babu *et al*., 2007; Ren *et al*., 2010; Sebald *et al*., 2010; Somphan *et al*., 2013). Therefore, investigating the dielectric properties of $ACu_3Ti_4O_{12}$ in detail will help explore the underlying physics behind the dielectric behaviors of CCTO. In this paper, we investigated the microstructure, dielectric, and electrical properties of $Eu_{2/3}Cu_3Ti_4O_{12}$ (ECTO), $Tb_{2/3}Cu_3Ti_4O_{12}$ (TCTO), and $Na_{1/2}Eu_{1/2}Cu_3Ti_4O_{12}$ (NECTO), together with the results of CCTO. Substituting for Ca decreased the dielectric constant and improved the loss tangent of CCTO. The possible reasons for the decreased dielectric response are discussed.

II. EXPERIMENTAL

$ACu_3Ti_4O_{12}$ ($A = Eu_{2/3}$, $Tb_{2/3}$, and $Na_{1/2}Eu_{1/2}$) (ACTO) and CCTO powders were synthesized by the conventional solid-state reaction method. High-purity Eu_2O_3, Tb_2O_3, Na_2CO_3, $CaCO_3$, CuO, and TiO_2 were weighed according to the stoichiometric ratios and mixed thoroughly in an agate mortar. The mixed powders were calcined in air at 1000 °C for 12 h and at 1100 °C for 24 h with an intermediate grinding. The calcined samples were milled and pressed into pellets of 5 mm in diameter and approximately 0.8 mm in thickness. The pellets were then sintered in air at 1100 °C for 20 h.

X-ray powder diffraction (XRD) data were recorded on an X-ray diffractometer (XRD-7000, SHIMADZU Limited) with Cu$K\alpha$ radiation and a diffracted-beam graphite monochromator operated at 40 kV and 40 mA. The XRD data were indexed using the DICVOL91 program (Boultif and Louër, 1991). The surface morphologies were obtained using an FEI, XL-30 scanning electronic microscopy (SEM) coupled with energy-dispersive spectrometer (EDS). To measure the dielectric properties, silver electrodes were painted on the samples' surfaces. Dielectric and complex impedance data were collected using an Agilent-4294A impedance analyzer with an AC

[a]Author to whom correspondence should be addressed. Electronic mail: limiao@xaut.edu.cn

voltage of 0.5 V. The measurements were performed between 293 and 473 K over the frequency range of 40 Hz–2.5 MHz.

III. RESULTS

The XRD patterns of CCTO and ACTO are shown in Figure 1. All the patterns can be indexed to a body-centered cubic cell (space group $Im\bar{3}$). This finding indicates that the doped ions do not cause any significant changes in the crystal structure. Notably, the diffraction peaks of ACTO shift toward high angles compared to CCTO (see the inset of Figure 1), indicating the change in the lattice constant (Chen *et al.*, 1995; Chen and Eysel, 1999). The indexed lattice parameters of ACTO are 7.38914(15) Å (ECTO), 7.38406(10) Å (TCTO), and 7.39140(10) Å (NECTO), which shrink compared to that of CCTO (7.39397(11) Å); this is due to the smaller ionic radii of Eu^{3+} ($r = 0.95$ Å), Tb^{3+} ($r = 0.92$ Å), and Na^{+} ($r = 0.95$ Å) than Ca^{2+} ($r = 0.99$ Å), and vacancies existed on the Ca site in ECTO and TCTO (the *A* sites are one-third vacant in order to achieve charge neutrality). Table I lists the observed and calculated *d* spacings and 2θ angles for CCTO and ACTO. In addition, no second phase is detected in the XRD patterns of ACTO. All these results show that Eu^{3+}, Tb^{3+}, or Na^{+} and Eu^{3+} together enter the lattice and substitute for Ca^{2+} (Chen *et al.*, 1997).

The microstructures of CCTO were examined with the SEM technique (see Figure 2). SEM showed the formation of irregularly shaped crystallites. Some grains of CCTO grew rapidly to sizes around 50 μm, indicating abnormal grain growth (Adams *et al.*, 2002; Chung *et al.*, 2004; Feng and Shiau, 2004). Moreover, a secondary liquid phase that crystallized between the grains was detected. To confirm the elemental compositions of the grains and the secondary liquid phase at grain boundaries, EDS spectra were acquired from the positions marked as #1 and #2 with two boxes. The EDS spectra of the grains showed the peaks corresponding to Ca, Cu, Ti, and O elements. The EDS spectra of the secondary liquid phase show that Cu peaks of the secondary liquid phase are much stronger than those of the grains. The analysis results of these two EDS spectra are listed in Table II. This finding indicates that the atomic percentage of the grains is nonstoichiometric, and Cu and O are deficient in the grain of CCTO. In the selected area of the secondary liquid phase, copper (48.46 at%) and oxygen (45.56 at%) were detected as the major components. It is reasonable to assume that this intergranular secondary liquid phase is CuO (or rich in CuO). However, we did not detect the CuO phase in XRD data; this may be because the amount of CuO was too little to be detected by the XRD technique. Further, a little amount of Ti (4.12 at%) and Ca (1.85 at%) was found to co-exist with copper and oxygen in the selected area of the secondary liquid phase.

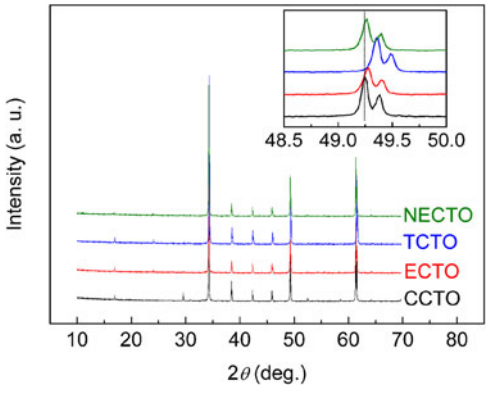

Figure 1. XRD patterns for CCTO, ECTO, TCTO, and NECTO. The inset is the expanded view of the XRD patterns in the 2θ range of 48.5°–50°.

TABLE I. List of indexes, *d* values, and 2θ of CCTO, ECTO, TCTO, and NECTO.

Sample	*h*	*k*	*l*	d_{obs} (Å)	d_{cal} (Å)	$2\theta_{obs}$ (°)	$2\theta_{cal}$ (°)
CCTO	1	1	0	5.22824	5.22966	16.945	16.940
	2	1	1	3.01912	3.01901	29.564	29.565
	2	2	0	2.61438	2.61449	34.272	34.270
	3	1	0	2.33850	2.33843	38.465	38.466
	2	2	2	2.13468	2.13467	42.305	42.305
	3	2	1	1.97636	1.97630	45.879	45.880
	4	0	0	1.84881	1.84865	49.246	49.251
	3	3	0	1.74285	1.74291	52.460	52.458
	4	2	2	1.50942	1.50938	61.371	61.373
	4	4	0	1.30713	1.30715	72.216	72.214
	4	3	3	1.26815	1.26812	74.807	74.809
	6	2	0	1.16911	1.16914	82.429	82.426
ECTO	1	1	0	5.22850	5.22972	16.944	16.940
	2	0	0	3.69612	3.69695	24.058	24.053
	2	2	0	2.61365	2.61362	34.282	34.282
	3	1	0	2.33778	2.33757	38.477	38.481
	2	2	2	2.13395	2.13382	42.320	42.323
	3	2	1	1.97566	1.97547	45.896	45.901
	4	0	0	1.84787	1.84784	49.273	49.274
	4	2	2	1.50869	1.50865	61.405	61.406
	4	4	0	1.30649	1.30647	72.257	72.258
	6	2	0	1.16845	1.16851	82.486	82.480
TCTO	1	1	0	5.21022	5.21119	17.004	17.001
	2	0	0	3.68669	3.68702	24.121	24.118
	2	2	0	2.60826	2.60821	34.355	34.355
	3	1	0	2.33308	2.33311	38.558	38.557
	2	2	2	2.13018	2.13000	42.399	42.402
	3	2	1	1.97216	1.97212	45.982	45.983
	4	0	0	1.84495	1.84485	49.356	49.359
	4	2	2	1.50655	1.50653	61.501	61.502
	4	4	0	1.30483	1.30481	72.363	72.364
	6	2	0	1.16709	1.16714	82.602	82.598
NECTO	2	0	0	3.69785	3.69780	24.047	24.047
	2	2	0	2.61426	2.61428	34.273	34.273
	3	1	0	2.33812	2.33818	38.471	38.470
	2	2	2	2.13451	2.13438	42.308	42.311
	3	2	1	1.97589	1.97600	45.890	45.888
	4	0	0	1.84836	1.84834	49.259	49.259
	4	2	2	1.50908	1.50907	61.387	61.387

The microstructures of ACTO are shown in Figure 3. The microstructure of ACTO was found to be different from that of CCTO as their grains have smooth faces associated with cubic appearance without the segregation of the Cu-rich phase at the grain boundaries. Moreover, the abnormal growth of the grain stops, and the grains become apparently uniform and fine. The largest grain of ACTO was about 10 μm. All these results indicate that Eu, Tb, and Na occupying the Ca site can induce significant changes in the microstructure. Such microstructure changes are considered to correlate closely with the absence of the CuO secondary phase (as discussed below).

The dielectric responses of CCTO and ACTO were investigated. The results are shown in Figure 4. Figure 4(a) presents the frequency-dependent dielectric responses at room temperature. It is apparent that the dielectric constants decreased after

https://doi.org/10.1017/S0885715619000769 Published online by Cambridge University Press

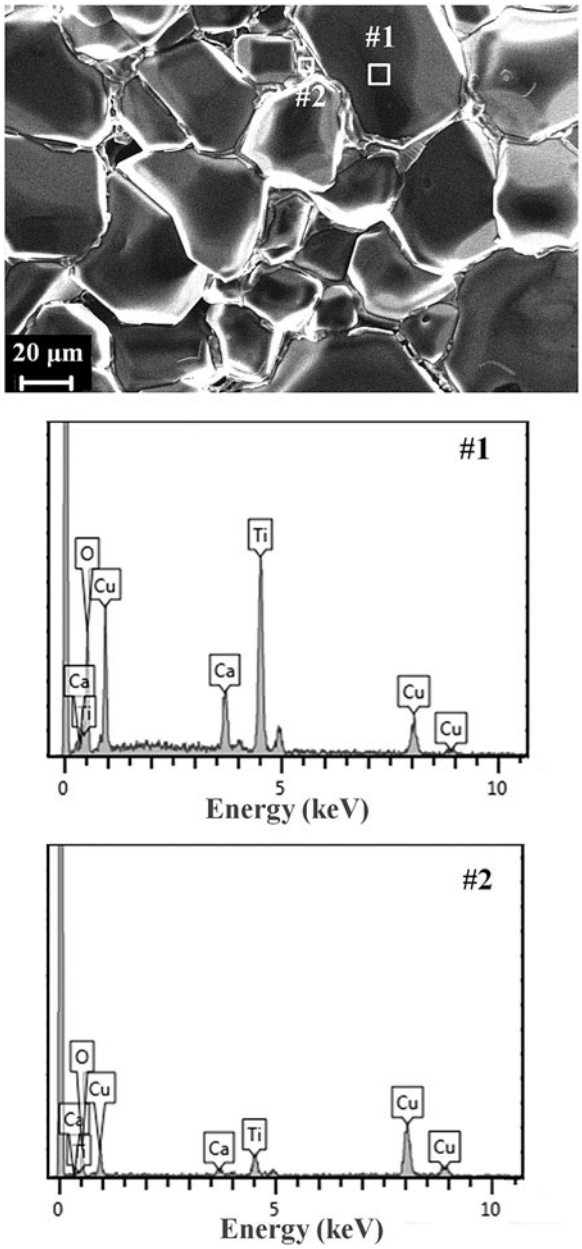

Figure 2. The SEM micrograph of CCTO and the corresponding EDS spectra.

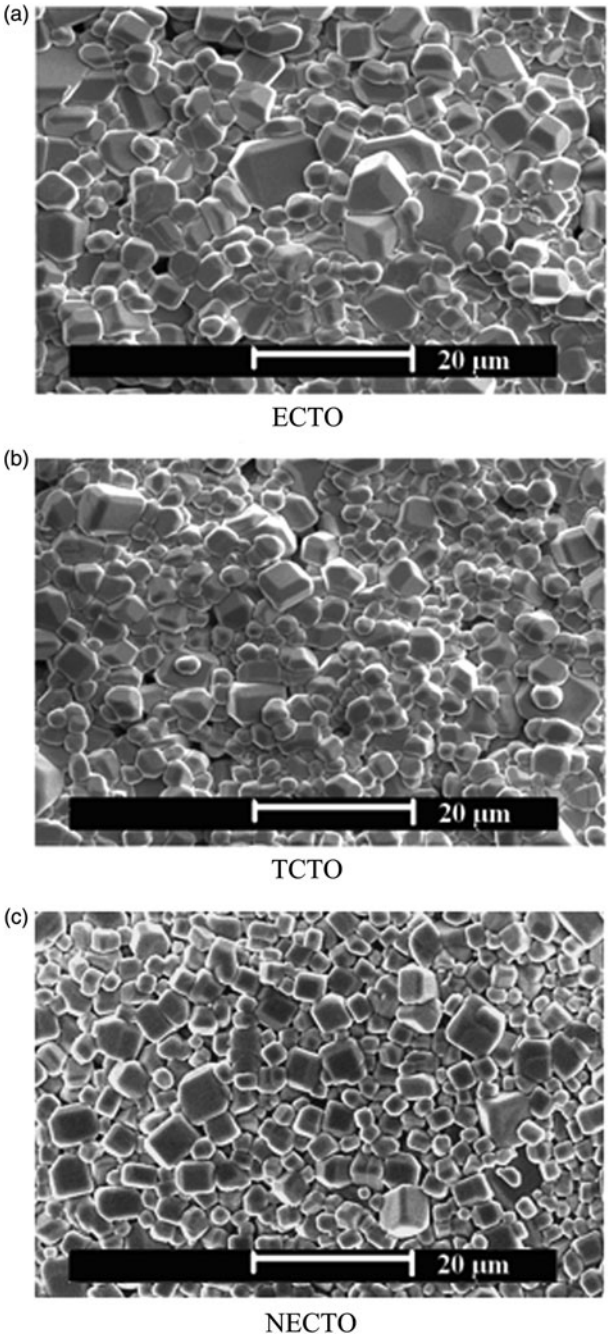

Figure 3. The SEM micrographs of ECTO (a), TCTO (b), and NECTO (c).

substitution on the Ca site. Notably, the loss tangent of the substituted samples also largely decreased compared to that of CCTO. The dielectric constants and loss tangents of the four samples at 1 kHz were about 10 400 and 0.182 (CCTO), 1200 and 0.058 (ECTO), 1500 and 0.042 (TCTO), and 2600 and 0.062 (NECTO), respectively. We can see that substituting on the Ca site reduces the loss tangent by more than 65% at 1 kHz. Although the dielectric constant also decreases, it still maintains a high magnitude of 10^3.

TABLE II. Atomic percentages (at%) of CCTO grain and the secondary phase obtained from their EDS spectra.

Locations	Ca (at%)	Cu (at%)	Ti (at%)	O (at%)
CCTO grain	6.86	16.71	28.02	48.41
Secondary phase	1.85	48.46	4.12	45.56

The temperature-dependent dielectric responses were investigated in the temperature range of 293–473 K [see Figure 4(b)]. The measurement frequency was 1 kHz. The CCTO sample was found to exhibit good temperature-independent dielectric constants below 360 K. Above 360 K, the dielectric constant rapidly increases with increasing temperature. The large increase in dielectric constant is accompanied with a loss tangent peak, indicating high-temperature relaxation was present in this sample (Grubbs *et al*., 2005; Lei and Chen, 2007; Li *et al*., 2017). Compared to CCTO, the dielectric constants of ACTO only slowly increased as the temperature increased, thus exhibiting good temperature-independent dielectric constants in the measured temperature range. The increments of dielectric constants in the temperature range of 293–473 K were about 380%, 250%, 170%, and 150% for CCTO,

https://doi.org/10.1017/S0885715619000769 Published online by Cambridge University Press

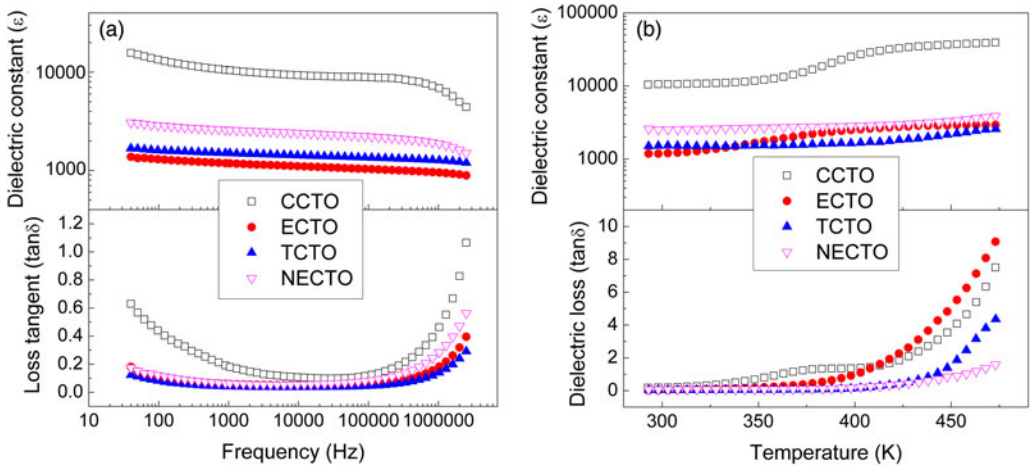

Figure 4. The frequency-dependent dielectric responses measured at room temperature (a) and temperature-dependent dielectric responses measured at 1 kHz (b) of CCTO, ECTO, TCTO, and NECTO.

ECTO, TCTO, and NECTO, respectively. In addition, no peaks were found in the loss tangent plots of ACTO. Thus, the samples of ACTO do not exhibit high-temperature dielectric relaxations. According to Grubbs *et al*. (2005) and Lei and Chen (2007), the high-temperature dielectric relaxation of CCTO is related to the oxygen vacancies or the oxygen vacancy-related point defect located at the grain boundary. The reduced high-temperature dielectric relaxation indicates the decrease in oxygen vacancies in the samples of ACTO.

To investigate the electrical properties of grain and grain boundary for CCTO and ACTO, the complex impedance plots measured at room temperature are presented in Figure 5. Steep inclines with nonzero intercepts at high frequency on the Z'-axis (see the inset of Figure 5) were observed for all the samples. The steep inclines are parts of semicircles representing the low-frequency grain boundary responses. It was reported that the diameters of the low-frequency semicircle correspond to the grain boundary resistances, whereas the high-frequency intercepts with the Z'-axis correspond to grain resistances. At room temperature, $R_{gb} \gg 5$ MΩ, $\omega_{max} < 40$ Hz, and therefore, only a small section of the grain boundary

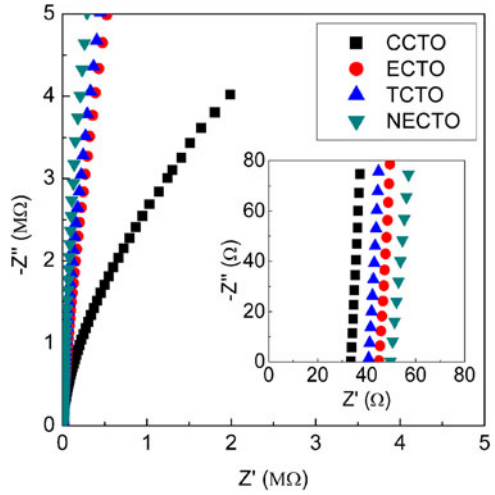

Figure 5. The complex impedance plots of CCTO, ECTO, TCTO, and NECTO measured at room temperature. The inset shows the expanded view of the high-frequency impedance data close to the origin.

semicircle is observed, as a steep incline at low frequencies. It is apparent that both the grain resistance and the grain boundary resistance increase by substituting on the Ca site. The increased grain boundary resistance may originate from the small grains of ACTO possessing large grain boundary area and/or the absence of the CuO secondary phase located at the grain boundary.

The complex impedance plots of ACTO were also investigated at different temperatures. The results are shown in Figure 6. With the increase in temperature, both the grain resistance and grain boundary resistance decreased. Conduction data of grain, σ, where $\sigma = 1/R$, were obtained by the nonzero intercepts of the complex impedance arcs and plotted against reciprocal temperature in Arrhenius format:

$$\sigma = \sigma_0 \exp(-E_a/k_B T) \quad (1)$$

where σ_0 is the prefactor, E_a is the activation energy for the relaxation, k_B is the Boltzmann constant, and T is the absolute temperature. Figure 7 shows the plots of log σ versus $1/T$, in which the solid lines are fitted results using Eq. (1). From the slopes of the fitted straight lines, we obtain the activation energy values of 0.45(5), 0.45(7), and 0.41(5) eV for the grain of ECTO, TCTO, and NECTO, respectively. These values were much larger than the reported values of 0.05–0.1 eV for the grain of CCTO (Homes *et al*., 2001; Chiodelli *et al*., 2004; Zhang and Tang, 2004), indicating the different conduction mechanism for the grain of ACTO. The activation energy of 0.05–0.1 eV for the grain of CCTO indicates that the electrons hopping accounts for grain conduction (Zhang and Tang, 2004). In our case, the activation energies of 0.41–0.45 eV for the grain of ACTO are in accordance with the ion jumping activation energy (0.2–1.0 eV) (Bidault *et al*., 1995). Therefore, substituting on the Ca site induces a change in the conducting mechanism of grain from electron hopping to ion jumping.

IV. DISCUSSION

The high-temperature dielectric relaxation illustrates the presence of oxygen vacancies in CCTO, which is confirmed

https://doi.org/10.1017/S0885715619000769 Published online by Cambridge University Press

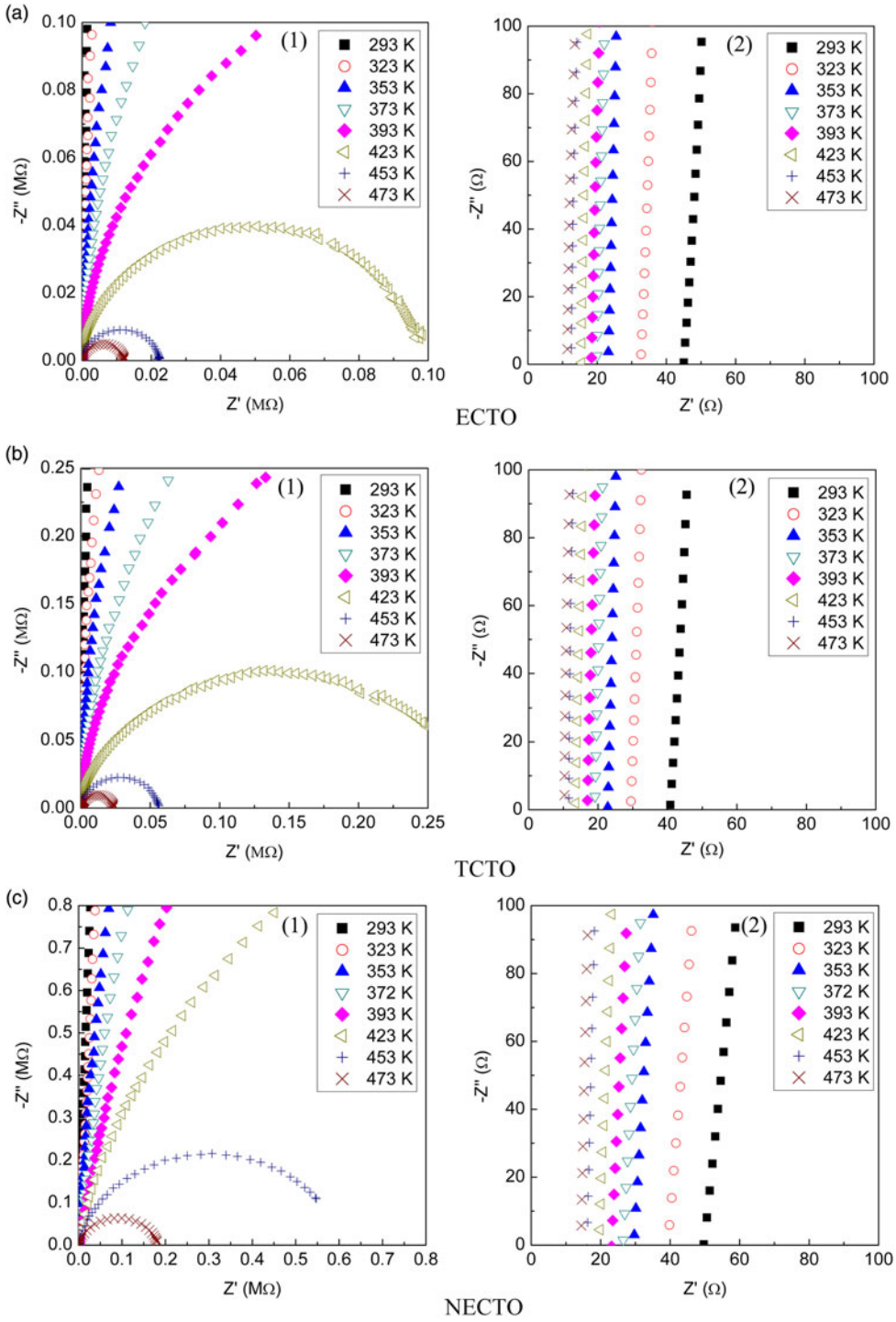

Figure 6. The complex impedance plots (1) and the expanded views of the high-frequency impedance data close to the origin (2) of ECTO (a), TCTO (b), and NECTO (c) measured at different temperatures.

by the EDS results that the grain of CCTO is oxygen-deficient. Oxygen vacancies arise from a small amount of oxygen loss during high-temperature sintering in the air, which is a common phenomenon in titanate-based perovskite at ≥1000 °C in the air (Morrison *et al.*, 2001). Oxygen loss from the lattice results in the generation of electrons according to:

$$O_0 \Leftrightarrow V_0^{\cdot\cdot} + 2e + \frac{1}{2}O_2 \qquad (2)$$

For carrier compensation, Cu ions are separated from the lattice to compensate the conduction electrons contributed by oxygen vacancies according to:

$$Cu_{Cu} + 2e \Leftrightarrow V''_{Cu} + Cu \qquad (3)$$

The departure of Cu ions leads to the formation of Cu vacancies in the lattice. These Cu ions mostly aggregate at grain boundaries and finally oxidize to CuO on cooling. The CuO phase in the oxide powder allows liquid-phase sintering and facilitates the grain growth (Sulaimain *et al.*, 2010;

https://doi.org/10.1017/S0885715619000769 Published online by Cambridge University Press

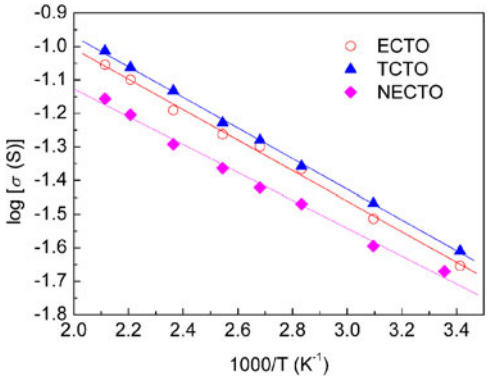

Figure 7. Arrhenius plots of grain conduction data for ECTO, TCTO, and NECTO.

Thongbai *et al*., 2012; Jesurani *et al*., 2013 ; Yuan *et al*., 2013a, 2013b; Senda *et al*., 2017). This finding is in accordance with our experimental results that CCTO with the CuO secondary phase located at the grain boundary possesses larger grains. However, for the samples of ACTO, the high-temperature dielectric relaxation is largely reduced, indicating the decrease in oxygen vacancies in the substituted samples. Furthermore, we did not observe any secondary phase located at the grain boundary. The absence of CuO secondary phase induces the decrease in the grain sizes of the substituted samples. According to the internal barrier layer capacitor (IBLC) model, the effective dielectric constant ϵ_{eff} can be represented by the following equation (West *et al*., 2004; Ni *et al*., 2006; Yuan *et al*., 2013b):

$$\varepsilon_{\text{eff}} = \varepsilon_{\text{r}}(t_{\text{g}}/t_{\text{gb}}) \tag{4}$$

where t_g is the grain average size, t_{gb} is the average thickness of the grain boundary layer, and ϵ_r is the relative dielectric constant of the grain boundary layer. Therefore, smaller grain average size will induce a lower dielectric constant. Because the grain sizes of ACTO largely decrease compared to CCTO, this may be a reason for the decrease in the dielectric constant of ACTO. Furthermore, the activation energy results indicate that the conducting mechanism for the grain of ACTO is ion jumping rather than electron hopping (which is for the grain of CCTO). The different carrier in grain may cause the different polarization form of the grain, which may also account for the decreased dielectric constant. In addition, the grain boundary plays an important role in the ceramic dielectric response due to giant barrier layer effects (Kim *et al*., 2008; Liu *et al*., 2009). The different grain boundary properties (e.g., absence of CuO secondary phase) may be another reason for the decreased dielectric constant of ACTO.

Therefore, the decreased dielectric constant of ACTO may be related to the decreased grain size, the different carrier in the grain, the different grain boundary properties, or a combination of these factors. Copper plays an important role in the decreased grain size and the different grain boundary properties, as the departure of copper from the lattice leads to the formation of the CuO secondary phase at the grain boundary and further induces abnormal grain growth. However, the departure of copper relies on the formation of oxygen vacancies according to Eqs. (2) and (3). Thus, both the factors of decreased grain size and the different grain boundary properties are associated with oxygen vacancies. According to Eq. (2), one oxygen vacancies can create two electrons, which contribute to the grain conduction of CCTO (Wang *et al*., 2002; Li *et al*., 2006). For the samples of ACTO, the amount of oxygen vacancies decreases. This may induce a different conduction mechanism for the grain. Furthermore, the decreased oxygen vacancies further decrease the content of Cu vacancies in the grain of ACTO [according to Eqs. (2) and (3)], which may also account for the different conduction mechanism for the grain of ACTO. In a word, the deficiency of oxygen vacancies may be a key reason for the decreased dielectric constant for the samples of ACTO. However, they remain high at values of 10^3. Further, the decrease in loss tangent may originate from the increase in the grain boundary resistance.

V. CONCLUSION

The microstructure, dielectric, and electrical properties of $ACu_3Ti_4O_{12}$ ($A = Eu_{2/3}$, $Tb_{2/3}$, and $Na_{1/2}Eu_{1/2}$) ceramics were investigated systematically. The results show that substituting for Ca decreases the loss tangent by more than 65% at 1 kHz, while largely improving the loss tangent of CCTO. Although the dielectric constant also decreases, it remains at a high magnitude of 10^3. The SEM measurements reveal that the mean grain size largely decreases by substituting for Ca and there is no CuO secondary phase located at the grain boundary in the samples of ACTO. The complex impedance measurements indicate that both the grain resistance and grain boundary resistance increase because of substituting for Ca. The activation energies of 0.41–0.45 eV for the grain of ACTO indicate that the conducting mechanism is ion jumping rather than electron hopping for the grain of CCTO. We speculate that the reduced dielectric constant of CCTO may be related to the decreased grain size, the different carrier in the grain, the different grain boundary properties, or a combination of these factors. All these factors are associated with the deficiency of oxygen vacancies in the samples of ACTO. The decrease in the loss tangent may be due to the increase in the grain boundary resistance.

SUPPLEMENTARY MATERIAL

The supplementary material for this article can be found at https://doi.org/10.1017/S0885715619000769.

FUNDING INFORMATION

This research was funded by Natural Science Basic Research Plan in Shaanxi Province of China (Program Nos.: 2019JQ-097 and 2018JQ1026), Scientific Research Program Funded by Shaanxi Provincial Education Department (Grant No. 17JK0548), and the Xi'an University of Technology.

Adams, T. B., Sinclair, D. C., and West, A. R. (**2002**). "Giant barrier layer capacitance effects in $CaCu_3Ti_4O_{12}$ ceramics," Adv. Mater. **14**, 1321–1323.

Babu, J. B., He, M., Zhang, D. F., Chen, X. L., and Dhanasekaran, R. (**2007**). "Enhancement of ferroelectric properties of $Na_{1/2}Bi_{1/2}TiO_3$-$BaTiO_3$ single crystals by Ce dopings," Appl. Phys. Lett. **90**, 102901.

Bidault, O., Maglione, M., Actis, M., and Kchikech, M. (**1995**). "Polaronic relaxation in perovskites," Phys. Rev. B. **52**, 4191–4197.

Boultif, A. and Louër, D. (**1991**). "Indexing of powder diffraction patterns for low-symmetry lattices by the successive dichotomy method," J. Appl. Crystallogr. **24**, 987–993.

Capsoni, D., Bini, M., Massarotti, V., Chiodelli, G., Mozzatic, M. C., and Azzoni, C. B. (**2004**). "Role of doping and CuO segregation in improving the giant permittivity of $CaCu_3Ti_4O_{12}$," J. Solid State Chem. **177**, 4494–4500.

Chen, X. L. and Eysel, W. (**1999**). "Subsolidus phase relations in La_2O_3-Bi_2O_3-CuO," Powder Diffr. **14**, 274–275.

Chen, X. L., Liang, J. K., and Wang, C. (**1995**). "Effect of high-angle diffraction data on Rietveld structure refinement," Acta Phys. Sin. Ov. Ed. **4**, 259–267.

Chen, X. L., Bauernfeind, L., and Braun, H. F. (**1997**). "$Na_{0.5}La_{0.5}RuO_3$: structure and electronic properties," Phys. Rev. B. **55**, 6888–6895.

Chiodelli, G., Massarotti, V., Capsoni, D., Bini, M., Azzoni, C. B., Mozzati, M. C., and Lupotto, P. (**2004**). "Electric and dielectric properties of pure and doped $CaCu_3Ti_4O_{12}$ perovskite materials," Solid State Commun. **132**, 241–246.

Chung, S.-Y., Kim, I.-D., and Kang, S.-J. (**2004**). "Strong nonlinear current-voltage behaviour in perovskite-derivative calcium copper titanate," Nat. Mater. **3**, 774–778.

Fang, T. T. and Liu, C. P. (**2005**). "Evidence of the internal domains for inducing the anomalously high dielectric constant of $CaCu_3Ti_4O_{12}$," Chem. Mater. **17**, 5167–5171.

Feng, T.-T. and Shiau, H.-K. (**2004**). "Mechanism for developing the boundary barrier layers of $CaCu_3Ti_4O_{12}$," J. Am. Ceram. Soc. **87**, 2072–2079.

Grubbs, R. K., Venturini, E. L., Clem, P. G., Richardson, J. J., Tuttle, B. A., and Samara, G. A. (**2005**). "Dielectric and magnetic properties of Fe- and Nb-doped $CaCu_3Ti_4O_{12}$," Phys. Rev. B. **72**, 104111.

He, L., Neaton, J. B., Cohen, M. H., and Vanderbilt, D. (**2002**). "First-principles study of the structure and lattice dielectric response of $CaCu_3Ti_4O_{12}$," Phys. Rev. B. **65**, 214112.

Homes, C. C., Vogt, T., Shapiro, S. M., Wakimoto, S., and Ramirez, A. P. (**2001**). "Optical response of high-dielectric-constant perovskite-related oxide," Science. **293**, 673–676.

Homes, C. C., Vogt, T., Shapiro, S. M., Wakimoto, S., Subramanian, M. A., and Ramirez, A. P. (**2003**). "Charge transfer in the high dielectric constant materials $CaCu_3Ti_4O_{12}$ and $CdCu_3Ti_4O_{12}$," Phys. Rev. B. **67**, 092106.

Jesurani, S., Kanagesan, S., Hashim, M., and Ismail, I. (**2013**). "Dielectric properties of Zr doped $CaCu_3Ti_4O_{12}$ synthesized by sol-gel route," J. Alloys Comp. **551**, 456–462.

Kim, K.-M., Lee, J.-H., Lee, K.-M., Kim, D.-Y., Riu, D.-H., and Lee, S. B. (**2008**). "Microstructural evolution and dielectric properties of Cu-deficient and Cu-excess $CaCu_3Ti_4O_{12}$ ceramics," Mater. Res. Bull. **43**, 284–291.

Lei, N. and Chen, X. M. (**2007**). "Dielectric relaxations and formation mechanism of giant dielectric constant step in $CaCu_3Ti_4O_{12}$ ceramics," Appl. Phys. Lett. **91**, 122905.

Li, M., Feteira, A., Sinclair, D. C., and West, A. R. (**2006**). "Influence of Mn doping on the semiconducting properties of $CaCu_3Ti_4O_{12}$ ceramics," Appl. Phys. Lett. **88**, 232903.

Li, M., Liu, Q., and Li, C. X. (**2017**). "Study of the dielectric responses of Eu-doped $CaCu_3Ti_4O_{12}$," J. Alloys Comp. **699**, 278–282.

Liu, J. J., Duan, C.-G., Yin, W.-G., Mei, W. N., Smith, R. W., and Hardy, J. R. (**2004**). "Large dielectric constant and Maxwell-Wagner relaxation in $Bi_{2/3}Cu_3Ti_4O_{12}$," Phys. Rev. B. **70**, 144106.

Liu, J. J., Duan, C.-G., and Mei, W. N. (**2005**). "Dielectric properties and Maxwell-Wagner relaxation of compounds $ACu_3Ti_4O_{12}$ (A=Ca, $Bi_{2/3}$, $Y_{2/3}$, $La_{2/3}$)," J. Appl. Phys. **98**, 093703.

Liu, L. J., Fan, H. Q., Chen, X. L., and Fang, P. Y. (**2009**). "Electrical properties and microstructural characteristics of nonstoichiometric $CaCu_{3x}Ti_4O_{12}$ ceramics," J. Alloys Comp. **469**, 529–534.

Morrison, F. D., Sinclair, D. C., and West, A. R. (**2001**). "An alternative explanation for the origin of the resistivity anomaly in La-doped $BaTiO_3$," J. Am. Ceram. Soc. **84**, 474–476.

Ni, L., Chen, X. M., Liu, X. Q., and Hou, R. Z. (**2006**). "Microstructure-dependent giant dielectric response in $CaCu_3Ti_4O_{12}$ ceramics," Solid State Commun. **139**, 45–50.

Ren, H., Liang, P., and Yang, Z. (**2010**). "Processing, dielectric properties and impedance characteristics of $Na_{0.5}Bi_{0.5}Cu_3Ti_4O_{12}$ ceramics," Mater. Res. Bull. **45**, 1608–1613.

Sebald, J., Krohnsa, S., Lunkenheimer, P., Ebbinghaus, S. G., Riegg, S., Reller, A., and Loidl, A. (**2010**). "Colossal dielectric constants: a common phenomenon in $CaCu_3Ti_4O_{12}$ related materials," Solid State Commun. **150**, 857–860.

Senda, S., Rhouma, S., Torkani, E., Megriche, A., and Autret, C. (**2017**). "Effect of nickel substitution on electrical and microstructural properties of $CaCu_3Ti_4O_{12}$ ceramic," J. Alloys Comp. **698**, 152–158.

Sinclair, D. C., Adams, T. B., Morrison, F. D., and West, A. R. (**2002**). "$CaCu_3Ti_4O_{12}$: one-step internal barrier layer capacitor," Appl. Phys. Lett. **80**, 2153–2155.

Somphan, Z. W., Thongbai, P., Yamwong, T., and Maensiri, S. (**2013**). "High Schottky barrier at grain boundaries observed in $Na_{1/2}Sm_{1/2}Cu_3Ti_4O_{12}$ ceramics," Mater. Res. Bull. **48**, 4087–4092.

Subramanian, M. A. and Sleight, A. W. (**2002**). "$ACu_3Ti_4O_{12}$ and $ACu_3Ru_4O_{12}$ perovskites: high dielectric constants and valence degeneracy," Solid State Sci. **4**, 347–351.

Subramanian, M. A., Li, D., Duan, N., Reisner, B. A., and Sleight, A. W. (**2000**). "High dielectric constant in $ACu_3Ti_4O_{12}$ and $ACu_3Ti_3FeO_{12}$ phases," J. Solid State Chem. **151**, 323–325.

Sulaimain, M. A., Hutagalung, S. D., Ain, M. F., and Ahmad, Z. A. (**2010**). "Dielectric properties of Nb-doped $CaCu_3Ti_4O_{12}$ electroceramics measured at high frequencies," J. Alloys Comp. **493**, 486–492.

Thongbai, P., Putasaeng, B., Yamwong, T., and Maensiri, S. (**2012**). "Modified giant dielectric properties of samarium doped $CaCu_3Ti_4O_{12}$ ceramics," Mater. Res. Bull. **47**, 2257–2263.

Wang, C. C. and Zhang, L. W. (**2007**). "Polaron relaxation related to localized charge carriers in $CaCu_3Ti_4O_{12}$," Appl. Phys. Lett. **90**, 142905.

Wang, W. Y., Zhang, D. F., Xu, T., Li, X. F., Zhou, T., and Chen, X. L. (**2002**). "Nonlinear electrical behavior and dielectric properties of (Ca, Ta)-doped TiO_2 ceramics," J. Alloys Comp. **335**, 210–215.

West, A. R., Adams, T. B., Morrison, F. D., and Sinclair, D. C. (**2004**). "Novel high capacitance materials: $BaTiO_3$: La and $CaCu_3Ti_4O_{12}$," J. Eur. Ceram. Soc. **24**, 1439–1448.

Yuan, W. X., Wu, Q. X., Liu, C. K., Luo, Z. K., and Li, Z. J. (**2013a**). "Effect of phase purity on dielectric properties of $CaCu_{3+x}Ti_4O_{12}$ ceramics," Solid State Sci. **24**, 58–61.

Yuan, W. X., Luo, Z. K., and Wang, C. D. (**2013b**). "Investigation on effects of CuO secondary phase on dielectric properties of $CaCu_3Ti_4O_{12}$ ceramics," J. Alloys Comp. **562**, 1–4.

Zhang, L. and Tang, Z.-J. (**2004**). "Polaron relaxation and variable-range-hopping conductivity in the giant-dielectric-constant material $CaCu_3Ti_4O_{12}$," Phys. Rev. B. **70**, 174306.

Zhang, J. L., Zheng, P., Wang, C. L., Zhao, M. L., Li, J. C., and Wang, J. F. (**2005**). "Dielectric dispersion of $CaCu_3Ti_4O_{12}$ ceramics at high temperatures," Appl. Phys. Lett. **87**, 142901.

https://doi.org/10.1017/S0885715619000769 Published online by Cambridge University Press